ISPRS Journal of Photogrammetry and Remote Sensing 104 (2015) 30–43

Contents lists available at ScienceDirect

ISPRS Journal of Photogrammetry and Remote Sensing

journal homepage: www.elsevier.com/locate/isprsjprs

A graph-based segmentation algorithm for tree crown extraction using airborne LiDAR data

Victor F. Strîmbu [a,*], Bogdan M. Strîmbu [b,c]

[a] Department of Ecology and Natural Resource Management, Norwegian University of Live Sciences, Høgskoleveien 12, 1430 Ås, Norway
[b] School of Forestry, Louisiana Tech University, 1501 Reese Dr., Ruston, LA 71272, USA
[c] Forest Research and Management Institute, 128 Bd. Eroilor, Voluntari, IF 077190, Romania

ARTICLE INFO

Article history:
Received 20 July 2014
Received in revised form 23 January 2015
Accepted 25 January 2015
Available online 19 March 2015

Keywords:
Individual tree crown (ITC)
Hierarchical data structure
Directed acyclic graph (DAG)
Aerial laser scan (ALS)
Resource estimation

ABSTRACT

This work proposes a segmentation method that isolates individual tree crowns using airborne LiDAR data. The proposed approach captures the topological structure of the forest in hierarchical data structures, quantifies topological relationships of tree crown components in a weighted graph, and finally partitions the graph to separate individual tree crowns. This novel bottom-up segmentation strategy is based on several quantifiable cohesion criteria that act as a measure of belief on weather two crown components belong to the same tree. An added flexibility is provided by a set of weights that balance the contribution of each criterion, thus effectively allowing the algorithm to adjust to different forest structures.

The LiDAR data used for testing was acquired in Louisiana, inside the Clear Creek Wildlife management area with a RIEGL LMS-Q680i airborne laser scanner. Three 1 ha forest areas of different conditions and increasing complexity were segmented and assessed in terms of an accuracy index (AI) accounting for both omission and commission. The three areas were segmented under optimum parameterization with an AI of 98.98%, 92.25% and 74.75% respectively, revealing the excellent potential of the algorithm. When segmentation parameters are optimized locally using plot references the AI drops to 98.23%, 89.24%, and 68.04% on average with plot sizes of 1000 m^2 and 97.68%, 87.78% and 61.1% on average with plot sizes of 500 m^2.

More than introducing a segmentation algorithm, this paper proposes a powerful framework featuring flexibility to support a series of segmentation methods including some of those recurring in the tree segmentation literature. The segmentation method may extend its applications to any data of topological nature or data that has a topological equivalent.

1. Introduction

A key element in forest management is the correct assessment of the resources of interest at the start of the planning horizon. Using remotely sensed data in area-based resource estimation has been proved an effective and reliable alternative to traditional field sampling methodology (Hyyppä et al., 2000; Næsset, 1997, 2002). The rapid increase in sensor resolution and computational power, and decreasing data acquisition cost, renders automatic individual tree interpretation increasingly feasible. Characterization of the forest at the individual tree level not only enhances the traditional yet still dominant economical oriented forest inventory, but also extends its applications in disciplines where greater detail is valued, such as ecology, wildlife or biodiversity.

Obtaining individual tree information requires that trees are at least localized if not delineated in the remotely sensed data by an automated process. This task is not trivial and its difficulty stems in the level of detail present in the remotely sensed data, as well as limitations that have to do with the scale-space representation, the inherent lack of individualizing features in trees, the variability of tree crowns structure, and clumped crowns in dense forests.

With respect to the remote sensing data utilized, LiDAR scans became a preferred alternative, rapidly replacing the traditional optical imagery in tree segmentation applications (Jakubowski et al., 2013). When performed on optical imagery, the tree extraction process relies on the spectral contrast between tree crown pixels and background pixels, as well as tree crown illumination patterns. While the forest canopy surface may be reconstructed from optical imagery through stereopsis (Hirschmugl et al.,

* Corresponding author.
E-mail addresses: victor.strimbu@nmbu.no (V.F. Strîmbu), strimbu@latech.edu (B.M. Strîmbu).

http://dx.doi.org/10.1016/j.isprsjprs.2015.01.018
0924-2716/

2007), LiDAR data provides substantially more information with regards to vertical structure of the forest, a quality that recommended its use in this project.

Regardless of the remote sensing data type, a variety of tree detection and delineation algorithms have been proposed in the last two decades. Here we briefly survey those that often recur in the literature. Gougeon's valley following technique (Gougeon et al., 1992; Gougeon, 1989) is among the earliest attempts to tackle this problem. The algorithm starts at local minima and searches for adjacent pixels that lie in between pixels of higher value, with the resulting paths assumed to correspond to tree crown boundaries. Local maxima filtering (LMF) has been extensively employed in tree top detection with the aim to discriminate between true and spurious locations of tree tops (Dralle and Rudemo, 1996; Gebreslasie et al., 2011; Pitkänen, 2001; Popescu and Wynne, 2004; Wulder et al., 2000). When the entire tree crown extent is of interest, LMF is often used to provide seed points for algorithms that delineate entire tree crowns (Holmgren and Persson, 2004; Liu et al., 2013; Palenichka and Zaremba, 2007; Yu et al., 2011). Template matching segmentation methods rely on a generalized tree model. The choice of tree model varies from illumination patterns (Hung et al., 2012) to ellipses (Larsen and Rudemo, 1998), ellipsoids (Wolf and Heipke, 2007), Gaussian blobs (Brandtberg et al., 2003; Daliakopoulos et al., 2009; Pirotti, 2010), conic and parabolic surfaces (Persson et al., 2002; Tittmann et al., 2012). Region growing algorithms (Culvenor, 2002; Erikson, 2003; Hirschmugl et al., 2007) start with seed pixels and progressively grow regions by iteratively including adjacent pixels until a threshold of expansion or stopping criteria are met. Watershed segmentation (Bottai et al., 2013; Kwak et al., 2007; Tang et al., 2007) is a particular instance of region growing that operates on topologically inverted data by the analogy of pouring water in the local minima, and considering the basins limits as the water level rises. Clustering algorithms have been employed at pixel level (Gupta et al., 2010), voxel level (Reitberger et al., 2009) and subsegment level (Lee et al., 2010). Finally, global optimization algorithms segment trees simultaneously in an iterative process with the aim to reach a state of fitness for the segmented forest as a whole. Horváth et al. (2006) modeled the tree crown distribution in a forest with a "gas of circles" and Zhang and Sohn (2010) utilized a Markov Random Field model to optimize the spatial configuration of the trees. Regardless of the underlying segmentation algorithm, some authors have emphasized the scale space aspect either explicitly by locally adaptive methods (Palenichka et al., 2013; Popescu and Wynne, 2004), or implicitly by using a localized image processing treatment established by scale approximation techniques such as granulometry (Heinzel et al., 2011), multi-scale analysis (Skurikhin et al., 2013) or area-based stem number approximation (Ene et al., 2012).

While most of the above mentioned methods have reported relatively satisfactory performance, an international benchmarking project (Kaartinen et al., 2012) revealed however, that when applied to the same dataset, nine tested methods showed a high variability in their performance. In fact, the methods did not perform much better and often worse than simple local maxima and watershed based methods implemented by the authors of the report. In another comparative study, Larsen et al. (2011) compared the accuracy of six segmentation methods when applied to six different forest types. The algorithms were fundamentally different and were based on: local maxima filtering, valley following, region growing, template matching, scale-space theory, and stochastic processes. The results revealed that while all methods were relatively accurate when applied to a young plantation, they performed significantly different on other forest types. For instance, the region growing algorithm outperformed all the methods in a mixed forest area as well as an area with high stem density but was particularly poor on areas with isolated trees. Isolated trees on the other hand, were best extracted by the template matching method. While the first study reveals that the method of segmentation is the main source of variability in segmentation accuracy, the second study goes further and shows that the methods behave differently when applied to certain forest types. In other words, they are inherently more or less appropriate to segment forests of certain structure. The inherent inability to adapt to various forest conditions sometimes stems in reliance on overly simplified assumptions regarding the structure of tree crowns and their layout in the forest. Tree crowns have an extremely complex structure that varies greatly from species to species as well as with the context in which they developed. For instance, when following a template matching approach, authors are constrained to either employ simple generalized models or design models that target a particular type of tree. In a more general sense, yet by similar reasoning, most segmentation methods envision and define the individual tree by rigid rules, metrics, models or processes.

We aim to address the shortcomings identified above by using hierarchized data structures and a weighted graph to construct an abstract representation of the forest that enables us to quantify logical and spatial relations between tree crown components. A system of weights for five different cohesion criteria is at the core of the method and provides an effective way to accommodate different forest structures. While our solution consists in partitioning the weighted graph, the proposed graph based forest representation may be used as framework to implement a wide variety of segmentation algorithms.

2. Methods

2.1. Study area and LiDAR data

The LiDAR data were recorded in Vernon Parish, Louisiana, within Clear Creek Wildlife management area (Fig. 1). The forest vegetation in the area is dominated by pine species, predominantly loblolly pine (*Pinus taeda* L.), shortleaf pine (*Pinus echinata* Mill.), and longleaf pine (*Pinus palustris* Mill). Throughout the region

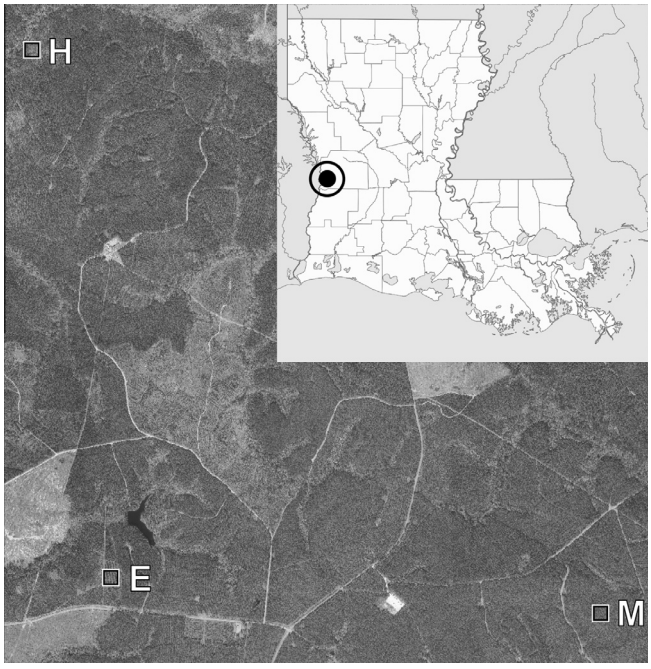

Fig. 1. Clear Creek Wildlife management area within Louisiana. The three 1 ha study areas are marked on the map with E – easy, M – medium, and H – hard.

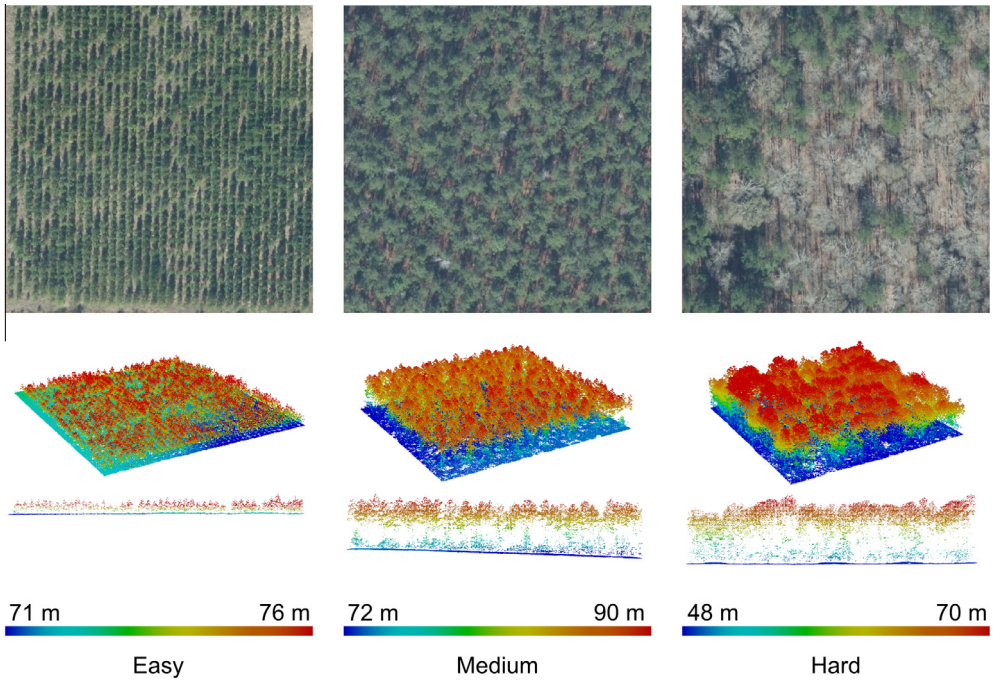

Fig. 2. Aerial photographs and LiDAR point clouds for the three study areas. The height scale is relative to the sea level.

Table 1
Dendrometric properties for the three areas. The forest layers are denoted: LL – lower layer, IL – intermediate layer, UL – upper level. The hard area is uneven aged, therefore only the age of the oldest trees is reported here. Species are abbreviated: Pinus taeda L. (PT), Pinus palustris Mill. (PP), Quercus falcata Michx. (QF), Quercus alba L. (QA), Liquidambar styraciflua L. (LS).

Area	LL	IL	UL	Total	hMax (m)	Height SD (m)	Age (years)	Species composition
Easy	137	864	379	1380	6.64	1.07	6	PT (100%)
Medium	0	36	390	426	19.94	1.54	23	PT (100%)
Hard	1	36	169	206	24.24	3.08	63	PP (33%), PT (4%), QF (27%), QA (31%), LS (5%)

hardwood species are encountered, likely confined to riparian areas, where various oaks (*Quercus* sp.), alders (*Alnus* sp.), poplars (*Populus* sp.), or sweetgums (*Liquidambar styracifula*) are present. The site index varies according with the species, but for the main economic species it is between 20 m and 30 m.

The LiDAR scan was conducted in February 2013 with a RIEGL LMS-Q680i scanner, equipped with digital full waveform sensor. The point cloud was created by processing the full waveform data with RiPROCESS v1.5.7. An average pulse density of 10/m^2, lead to an average of 30 Pts/m^2 in the point cloud after full waveform decomposition with RiANALYZE v5.4.1. To test the performance of the algorithm under different forest conditions of increasing complexity, three 1 ha areas were selected, each representing a typical situation that can be encountered in resource estimation (Fig. 2). The first area, labeled henceforth as "easy", is a young plantation forest, and is representative for a situation when the forest is very homogeneous in respect to dendrometric attributes, such as height, diameter and species. The second area, labeled henceforth as "medium", is a planted forest that reached the maturity stage, characterized by larger variability, despite that most of the dendrometric attributes are similar (e.g., species and age). The third area, labeled henceforth as "hard", represents a natural forest with minimum or no human intervention, characterized by low stem density, clustered spatial distribution, and large variability in both species and dendrometric attributes. The hard area is part of an uneven-age stand, characterized by an exponential distribution with respect to size. To enable accuracy assessment with respect to forest height layers, the reference trees in each area are partitioned in three layers. If hMax denotes the average height of the tallest 100 trees for a certain study area, then the lower layer consists in trees with heights less than 50% of hMax, the intermediate layer with heights between 50% and 80% of hMax, and the upper layer with trees taller than 80% of hMax. The number of trees in each layer and other dendrometric attributes are summarized for each area in Table 1, and a more detailed height distribution is illustrated in Fig. 3.

2.2. Segmentation method

2.2.1. Outline

While this section provides a global perspective of the segmentation procedure, individual steps are further explained in subsequent sections.

As part of the preprocessing stage, a grey-level image (Fig. 4-b) is created by discretizing the raw LiDAR point cloud horizontally, by a certain pixel size, and vertically by a predefined number of height levels. Adjacent pixels of the same value are grouped together to form patches (Fig. 4-c), and adjacent patches are organized hierarchically, based on their height (Fig. 4-d). At the top of each hierarchy stands a single patch, called root patch, identifying a local maximum. The spatial data is thus organized in an extensive directed acyclic graph (DAG), with nodes encoding patches. Within this structure, each hierarchy consists of all the patches that are reachable from the root patch, and will be looked upon as a logical entity that equates to a tree crown component. A higher level graph is constructed with nodes representing hierarchies and

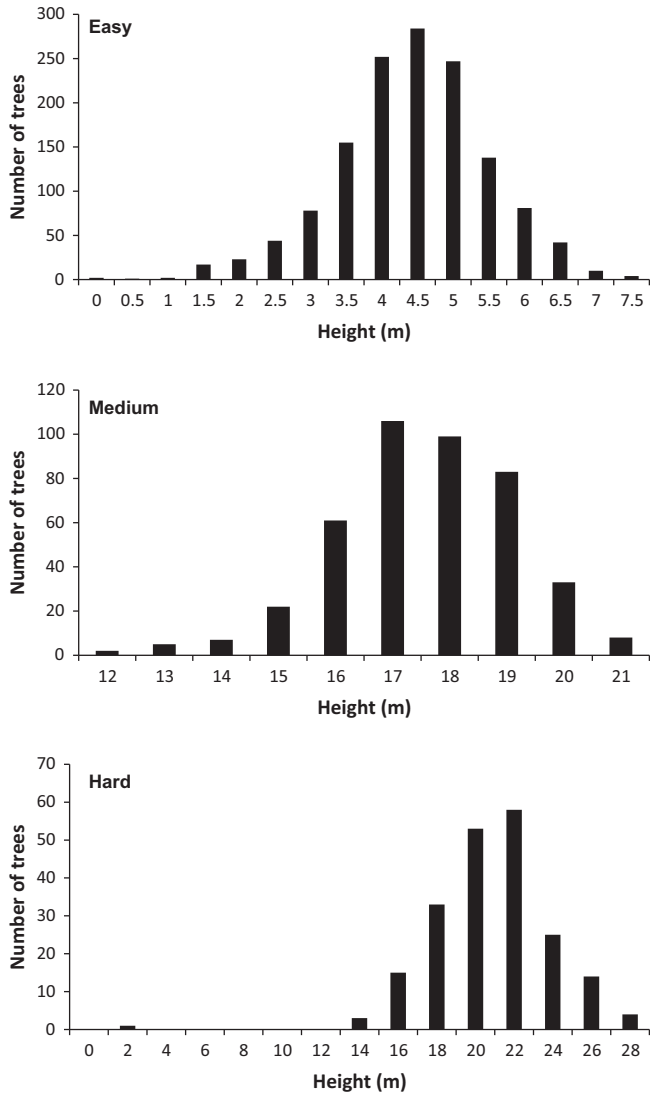

Fig. 3. Height distribution of reference trees in each area.

edges between any two hierarchies that have patches in common (Fig. 4-e). Edge orientation is set from the highest hierarchies (i.e., a hierarchy is considered to have the height of its root patch) to the lower ones, and their weights quantify the cohesion between two hierarchies. Each edge weight is calculated as a weighted average of five different cohesion criteria scores based on logical, quantitative, and spatial relations between the sets of patches within the ranks of two interconnected hierarchies. The graph constructed by these rules is also a DAG, property that facilitates its partition through edge elimination. Pruning all the non-maximal inbound edges as well as those weighted below an established threshold, effectively partitions the graph into connected components (Fig. 4-f) that group together highly cohesive hierarchies. The constituting pixels of each partition (Fig. 4-g) span crowns of individual trees and may be mapped back to the point cloud (Fig. 4-h) for further analysis.

2.2.2. Preprocessing

The raw LiDAR point cloud data is rasterized by overlapping a horizontal grid and recording the highest point in each cell. Beyond scale-space considerations (Hengl, 2006), the choice of the grid cell size must be observant to the LiDAR scanning density, aiming to capture sufficient detail, and in the same time avoid raster gaps. In terms of vertical discretizing, the space is divided into a predefined number of height levels, again aiming to capture sufficient vertical information but avoiding excessive noise.

Even with careful selection of the pixel size and the number of height levels, the raster is bound to have noise and empty pixels. To mitigate this problem the image is convoluted with a 3×3 Gaussian kernel that approximates the Gaussian blob:

$$G_\sigma(x,y) = \frac{1}{2\pi\sigma^2} e^{-\frac{\left(x^2+y^2\right)}{2\sigma^2}} \quad (1)$$

The Gaussian filter has a smoothing effect with the standard deviation (σ) acting as a magnitude parameter.

In another preparatory procedure, cells representing ground and sub arboreal vegetation are eliminated by establishing a height threshold. For each area, the appropriate threshold is selected by analyzing the height histogram of the LiDAR points (Fig. 5). In general, the height data should be normalized prior to elevation thresholding, but since all three study areas were relatively flat, normalization was not necessary.

2.2.3. Hierarchical structuring

The hierarchization stage structures the data in an extensive DAG that encodes the topological structure of the forest. Initially, cell patches are formed by adjacent cells of the same value (Fig. 6). The adjacency rule can be either 4-way or 8-way with the first being more appropriate when the number of height levels is low and the cell size is large as it lowers the risk of connecting regions pertaining to different trees.

Once the patches are created, the hierarchical structure is formed with the rule that every patch is a parent to its adjacent patches of lower value (Fig. 7). Relating the patches in this manner generates a DAG structure, denoted herein as P-DAG (i.e., patch DAG), with the following properties:

- A patch may have any number of parents and children.
- A parent-less patch coincides with a local maximum and is said to be the root or top of its hierarchy. A hierarchy is said to have the height of its top patch.
- A hierarchy is uniquely identified by its root node as the hierarchy consists of all the nodes that can be reached starting from this node.
- One patch may belong to more than one hierarchy. This property is especially prominent among the lower level patches.
- We will call cohesive any two hierarchies with interconnected structures (i.e., that have patches in common). Fig. 7 illustrates five cohesive pairs: (H1, H2), (H1, H3), (H2, H3), (H2, H4) and (H3, H4). The next section describes a way to quantify these relations.

2.2.4. Weighted graph

At this stage, hierarchies are treated as entities themselves, and a weighted DAG is formed with nodes corresponding to hierarchies and edges connecting cohesive pairs of hierarchies (Fig. 8). This higher level structure will be denoted as H-DAG (i.e., hierarchy DAG).

Edge orientation is set from higher hierarchies to lower ones. When the two related hierarchies are of the same height, the following properties are used in this order: the total number of cells spanned by each hierarchy, the number of cells in the top patches and the relative position of the two hierarchy tops. The last property will secure a consistent orientation when the previous measures are equal in order to avoid graph cycles.

Calculating the H-DAG edge weights is central to the segmentation algorithm. The weights must score the spatial relations of tree canopy elements in the forest. Consequently, H-DAG nodes belonging to the same tree should be connected by greater weights

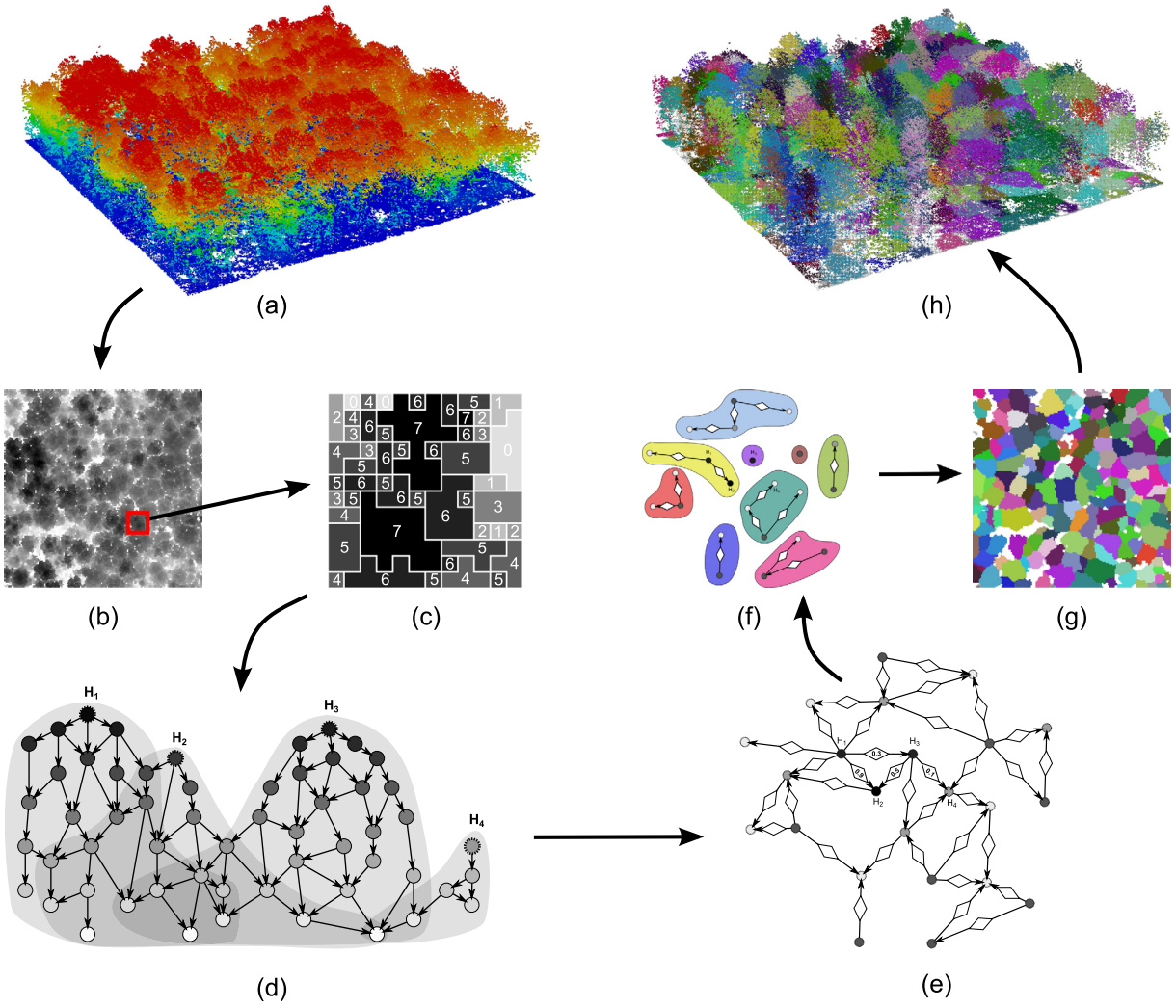

Fig. 4. Overview of the segmentation method: (a) the initial LiDAR point cloud, (b) height raster image, (c) patches formed with adjacent cells of the same value, (d) hierarchized patches, (e) weighted graph, (f) graph partition, (g) partition result on the raster, (h) segmented point cloud.

compared to weights connecting elements of separate trees. The H-DAG weights are computed based on five different properties that we call cohesion criteria: level depth (LD), node depth (ND), shared ratio (SR), top distance (TD) and centroid distance (CD). Scores for each of these criteria are calculated as real numbers between 0 and 1 and are an expression of how strongly each of the criteria supports the belief that two hierarchies are components of the same tree. The following paragraphs explain the criteria, the intuition behind them, as well as how their respective scores are calculated.

Level depth (LD) represents the minimum number of height levels between one of the two hierarchy tops and a contact patch (i.e., a node with parents in both hierarchies). The intuition behind the LD criterion is that lower values translate to shallow rifts between hierarchies, and consequently, an increased probability that the hierarchies belong to the same tree. The LD score between two connected hierarchies x and y is calculated by

$$S_{\mathrm{LD}}(x,y) = \frac{1}{\min_{r\in\{r_x,r_y\},i\in H_x,i\in H_y} dh(r,i)} \tag{2}$$

where r_x is the root node, H_x is the set of nodes of hierarchy x and $dh(r,i)$ is the difference in height levels between nodes r and i.

Node depth (ND) is similar to the level depth but considers the minimum number of nodes necessary to reach a contact patch from either hierarchy top. It complements the level depth by allowing deeper rifts between two hierarchies that are otherwise close to each other. The associated score is calculated by

$$S_{\mathrm{ND}}(x,y) = \frac{1}{\min_{r\in\{r_x,r_y\},i\in H_x,i\in H_y} dn(r,i)} \tag{3}$$

where $dn(r,i)$ calculates the path length in number of nodes between P-DAG nodes r and i.

Shared ratio (SR) calculates the number of cells of all the shared patches as a proportion of the total number of cells spanned by the two hierarchies. It is expected that a higher SR correlates with hierarchies of relatively close heights that may represent symmetrical branches of the same trees. Its score equates to the ratio:

$$S_{\mathrm{SR}}(x,y) = \frac{|Cell\_Set(H_x \cap H_y)|}{|Cell\_Set(H_x \cup H_y)|} \tag{4}$$

Top distance (TD) measures the horizontal distance between the top patches of the two hierarchies. If a top patch has more than one cell, its centroid is considered instead. The closer two hierarchy tops are, the higher the chance of belonging to the same tree. The associated score is inverse proportional to the calculated distance:

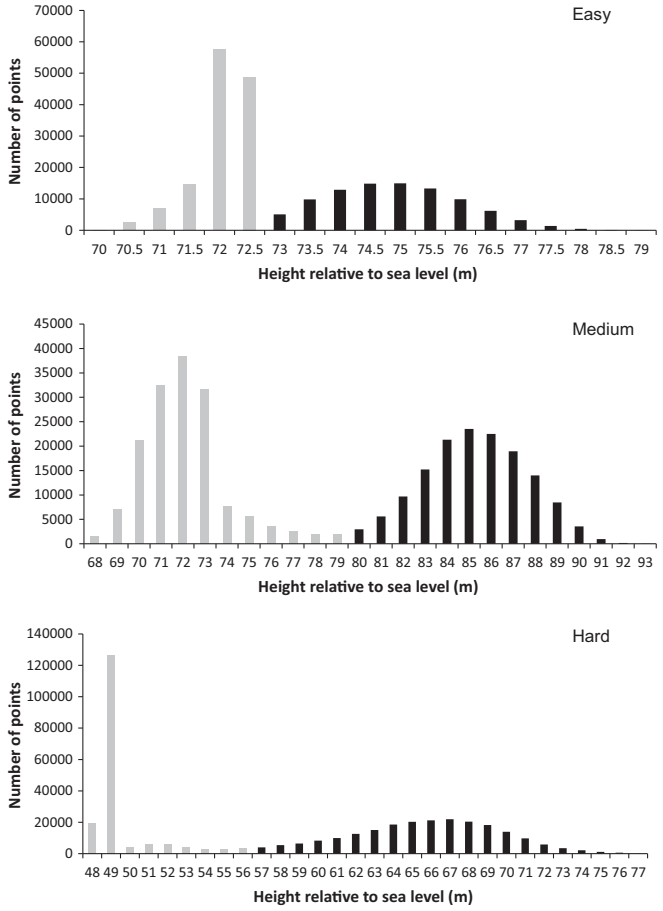

Fig. 5. LiDAR point height distribution for the three areas. Points within the grey height intervals have been eliminated.

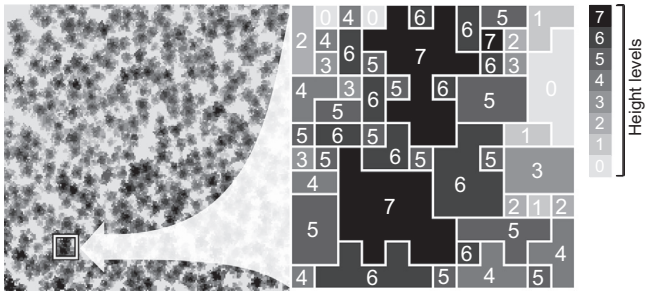

Fig. 6. Equal-height patches are formed by adjacent cells. Here the medium area point cloud is discretized on eight height levels and patches are formed by the four-way adjacency rule.

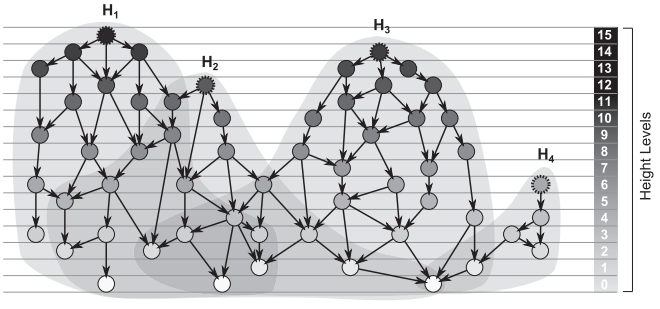

Fig. 7. Hierarchical organization of patches: P-DAG. Here are illustrated four interconnected hierarchies labeled H_1 to H_4 with nodes on 16 height levels.

$$S_{\mathrm{TD}}(x,y) = \frac{1}{C(r_x) - C(r_y)} \tag{5}$$

Centroid distance (CD) measures the distance between two hierarchies using their height adjusted centroids (HACs) instead of just the top. The HAC is calculated as a weighted mean of all the patch centroids, the weights being proportional to the patch size as well as its height level:

$$\mathrm{HAC}(x) = \frac{\sum_{p\in H_x} |Cell_{Set(p)}| \times (dh(r_x,p)+1) \times C(p)}{\sum_{p\in H_x} |Cell_{Set(p)}| \times (dh(r_x,p)+1)} \tag{6}$$

In this manner, the HAC is biased toward the hierarchy top but is also influenced by the lower layers in the hierarchy. CD compensates TD in situations when two trees lean toward each other, or for any other reason their tops are close but the rest of their crowns are divergent. The associated score is calculated by

$$S_{\mathrm{CD}}(x,y) = \frac{1}{\|\mathrm{HAC}(x) - \mathrm{HAC}(y)\|} \tag{7}$$

The total weight of an edge is calculated as a weighted mean of the five scores:

$$W(x,y) = \sum_{crt=\mathrm{LD,\ ND,\ SR,\ TD,\ CD}} W_{crt} \times S_{crt}(x,y) \tag{8}$$

A weighted mean is used under the assumption that not all criteria are equally significant. In particular, they may not be equally significant for a certain forest type. Key to an accurate segmentation is to balance the score weights in a way that fits the structure of the particular forest area under study.

2.2.5. Graph partitioning

Grouping tree crown components to form integral tree crowns equates to partitioning the H-DAG. The partitioning procedure isolates connected components in the graph by eliminating weak edges. Similar to parentless patches being hierarchy tops within the P-DAG, parentless or source nodes in H-DAG will represent tree tops. There are a certain number of source nodes that the H-DAG features prior to edge pruning. These can be looked upon as the minimum number of trees that the segmentation will produce considering that edge elimination-based partitioning generates additional source nodes. Edges are eliminated based on a weight threshold (WT) and by restricting the number of inbound edges to a maximum of one. If the set of week edges is defined as

$$\mathrm{WE} = \{(x,y) \in \text{H-DAG} | W(x,y) < WT\}$$

and the set of non-maximal inbound edges as

$$\mathrm{NMIE} = \{(x,y) \in \text{H-DAG} | \exists (z,y), W(x,y) < W(z,y)\}$$

then the set of edges to be eliminated is formed by the union $\mathrm{WE} \cup \mathrm{NMIE}$.

While thresholding is decisive to the number of partitions in the graph, non-maximal inbound edge elimination decides the membership of nodes accessible from multiple sources. The procedure essentially transforms the H-DAG into a forest both in the data structural sense and in the sense that it encodes the individual trees of the real forest. It is a simple and computationally efficient way (i.e. linear complexity) to partition a graph relying on the assumption that the underlying graph is acyclic.

2.2.6. Post-processing

Before final crown delineation is obtained, each pixel must be assigned to a unique tree. Despite the fact that at the H-DAG level hierarchies are separated, within the P-DAG structure, individual pixel patches located on the outskirts of the tree crowns may still belong to hierarchies from different partitions. In this scenario their membership is decided by proximity to a tree center. Lastly,

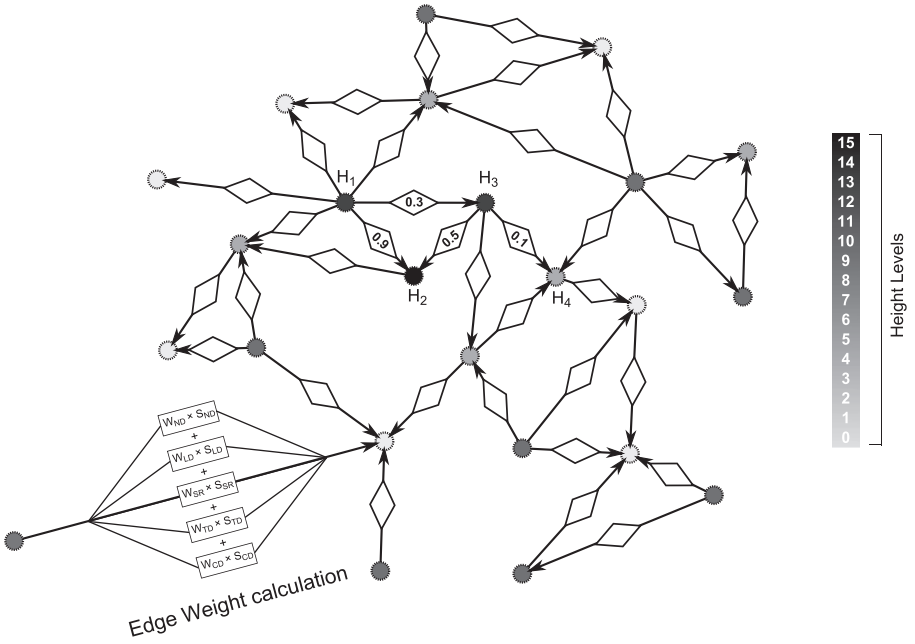

Fig. 8. H-DAG with nodes that encode individual hierarchies and edges that quantify cohesion. The four hierarchies from Fig. 6 are labeled here H_1 to H_4. On the bottom-left the edge weight calculation is decomposed.

the small segments are filtered out and the final segmentation result consists in disjoint sets of pixels that are mapped back to the point cloud.

2.3. Accuracy assessment

The actual position of the trees was determined by visual analysis of the LiDAR point cloud and the high resolution multispectral imagery (i.e., GSD of 15 cm). In most cases trees could be identified by inspecting the point cloud from different angles. Whenever discerning the trees became problematic, the stereographic visualization of multispectral images complemented the point cloud perspective, and assisted in the correct positioning of the trees.

The accuracy of a solution was assessed by counting the omissions (O) and commissions (C). In addition, the total number of errors $T = O + C$, as well as the omission–commission balance $B = |O–C|$ are considered when comparing segmentation results on the same forest area for parameter tuning purposes. While the total error reflects segmentation quality in general, it is sometimes desired to find a segmentation that produces a number of trees close to the ground reality, in which case the aim is to balance the omission and commission. With respect to the total number of trees (N), we report the results by the detection rate ($DR = (N - O)/N \times 100$) as well as an accuracy index ($AI = (N - O - C)/N \times 100$) Pouliot et al. (2002), penalized by both omission and commission.

An assessment tool was developed to automatically match the correctly identified trees. The position of each segmented tree is established as the location of the highest pixel in the set of pixels that make up the crown. The matching procedure pairs the closest reference tree location within a given radius for any segmented tree and then eliminates all the non-minimal pairs with the same reference tree. The search radius for the easy and medium areas was set to 3 pixels (0.9, 1.2 or 1.5 m, depending on pixel size) and for the hard area to 5 pixels (2, 2.5 or 3 m, depending on pixel size). A more permissive search radius was used for the hard area to allow tree top matching for some of the larger crowns. The omission set are those trees from the reference set that were not paired with any tree location from the segmented trees set. Conversely, those top locations in the segmentation set without a matching pair constitute the commission set.

2.4. Parameter space sampling

Proper parameterization is essential for quality segmentation. Scale-space parameters together with the algorithm specific parameters form a hyperspace of parameterization that is explored in search for regions that result in quality segmentation, revealing thus the algorithm's potential.

Rather than formulating a complicated and ultimately unfeasible search problem, a two phase sampling for a close to optimum set of parameter values was conducted. The first phase aimed to identify the most appropriate scale-space representation of each area as well as to narrow down the range of some parameters. In the second phase the results are refined by increasing the parameter sampling density. In each phase, a set of values is established for each parameter (Fig. 9) and all the possible combinations are tested, recording the afferent omission and commission every time. The total number of parameter value combinations for each area was 137,781 in the first phase and 400,000 in the second phase.

2.5. Practical approach to estimate the optimum parameters

In a real scenario the lack of ground truth for the entire forested area under study renders optimum parameterization impossible. Needless to say, tree segmentation itself is pointless in the context of already knowing the ground truth. Despite ground truth unavailability at the entire forest scope, sampled area plots are usually available in managed forests or may be synthetically produced by the means of photogrammetry. An experiment has been designed, aiming to evaluate the accuracy of tree segmentation with parameters estimated from individual area plots. Area plots entail the ground truth necessary to produce an optimum segmentation locally. If the forest area of interest is sufficiently homogenous, the parameters derived from tree segmentation in

		Parameter	Global tuning parameter values		Plot tuning parameter values
			Phase I	Phase II	
Preprocessing	Scale-space	LiDAR point height threshold (HT)	73^{E}, 80^{M}, 57^{H}		
		Cell size (CS)	$0.3^{E,M}$, 0.4, 0.5, 0.6^{H}	0.4^{E}, 0.5^{M}, 0.6^{H}	
		Height levels count (LC)	32, 64, 128	$64^{E,M}$, 128^{H}	64
		Gaussian standard deviation (σ)	0, 0.5, 0.6, ... , 1.0	0.6^{E}, 0.9^{M}, 1.0^{H}	
Segmentation		Cell neighborhood (CN)	8-way	4-way, 8-way	
	Core / Cohesion criteria	Level depth (LD)	0, 50, 100*	0, 25, 50, 75, 100*	0, 33, 66, 100*
		Node depth (ND)			
		Shared ratio (SR)			
		Top distance (TD)			
		Centroid distance (CD)			
		Edge weight threshold (EWT)	0.1, 0.2, ... , 0.9	$(0.30, 0.32, ... , 0.60)^{E,M}$ $(0.20, 0.22, ... , 0.50)^{H}$	0.10, 0.15, ... , 0.95
Post-processing		Crown area threshold (CAT)	1^{E}, 2^{M}, 5^{H}	$(0.64, 0.8, 0{,}96, 1.12)^{E}$ $(1.25, 1.75, 2.25, 2.75)^{M}$ $(7.2, 9, 10.8, 12.6)^{H}$	

E, M, H the parameter value was used exclusively for the easy, medium and hard areas respectively
* the set of cohesion criteria weights was subsequently normalized

Fig. 9. Parameter value sets used in parameter space sampling.

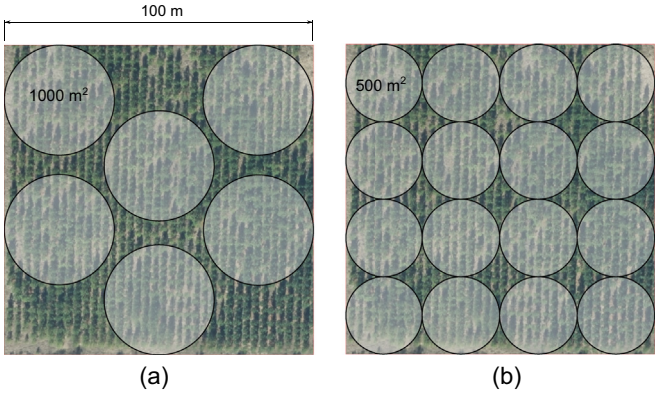

Fig. 10. Circular plots layout in the 1 ha study areas. Here the easy area overlay is shown. (a) 1000 m^2 plots, (b) 500 m^2 plots.

a certain plot may estimate the optimum parameterization globally. A similar approach was used by Forzieri et al. (2009) who used plot references to select the best among six watershed segmentation algorithms.

A set of 6 plots of 1000 m^2 and 16 plots of 500 m^2 were laid out within each area in a grid pattern as shown in Fig. 10. In total, 66 (6 + 16 = 22 per area) circular plots were cut out from the reference areas and each was segmented with 147,456 parameter combinations (Fig. 9). For each plot the parameter combination resulting in the best AI is recorded and then used in segmenting the entire 1 ha area.

T-tests were performed to formally assess whether the results with parameters estimated by plots are statistically different from the optimum results. Considering that t-test assumes unimodal, symmetrical distribution, Kolmogorov–Smirnov test was used to verify normality.

2.6. Cohesion criteria analysis

The cohesion criteria weights resulting in quality segmentations (i.e., the best 10 total errors) were preliminary assessed in search for patterns in their distributions. To this end, one way ANOVA initially tested the difference in criteria weight means between groups that yield different total errors. The separation of weights leading to significantly different results was performed using Bonferroni multiple comparisons test. The inference validity is secured by the large number of results within the best 10 total errors in each area: 25,000, 70,000, and 50,000 for the easy, medium and hard area, respectively.

To investigate the spectrum of associations between cohesion criteria, ANOVA was executed using the following linear model:

$$AI = LD|ND|SR + TD|CD$$

where AI is the accuracy index and "|" denotes factorial combination (e.g., $TD|CD = TD + CD + TD \times CD$, where $\times$ denotes the interaction between cohesion criteria). The two interaction terms were chosen to group criteria of similar nature: LD, ND and SR operate on the graph and TD and CD are simply Euclidian distances.

As ANOVA does not account for dependencies between cohesion criteria, MANOVA was conducted to identify sets of cohesion criteria that generate quality segmentations. The significance of the multivariate analysis of the cohesion criteria was assessed using Wilks' lambda. Rencher (1992) argued that interpretation of canonical variates that are not standardized either transforms multivariate analysis in univariate analysis (e.g., correlation between each attribute and the canonical variates) or reduces the optimality of the canonical correlation (e.g., rotation of the canonical variate coefficients). Therefore, the canonical variates were interpreted using the standardized coefficients, as recommended by Rencher (1992) and Hardle and Simar (2003). The canonical variates with variance

larger than 5% were selected for interpretation based on Noble et al. (2004) recommendation, and the attributes with canonical coefficients larger than 0.3 were considered part of the variate, as suggested by Tabachnick and Fidell (2001). The analysis was executed with SAS 9.3 (SAS Institute, 2010).

3. Results

The best AI obtained in the first phase parameter sampling for the easy, medium and hard images was 98.7%, 91.8%, and 73.3% respectively (Table 2), revealing that the optimum scale-space for each area differs in both cell size and Gaussian standard deviation. For the easy area CS = 0.4 m and σ = 0.6 yielded the best result, the medium area was best segmented with CS = 0.5 m and σ = 0.9, and the hard area with CS = 0.6 m and σ = 1. The second phase parameter sampling refined these results to AIs of 98.98%, 92.25%, and 74.75% for the three areas (Table 3). Although the relatively small increase in AI reveals that parameter tuning was sufficient in the first phase, subsequent inferences are based on the results obtained in the second phase. In Fig. 11 the best segmentation results are spatially visualized for each area.

As expected, the detection rates have an ascendant trend with respect to the forest height layers. However, the lack of representation for the lower layer in the medium and hard areas prohibits any inference on the algorithm performance in those strata as they were defined (i.e. trees with heights <50% of hMax). The detection rate for the lower, intermediate and upper layers in the easy area are 95%, 99.3% and 100% respectively. The forest layer seems to have a more significant impact on the detection rate for the medium and hard areas, where the detection rate reduces from the upper to the intermediate layer by 13% and 22% respectively (Table 3).

The cumulative distribution function of AI revealed that irrespective the accuracy measure, a plateau region is reached

Table 2
The best results in terms of AI in the first phase. The best result for each area is highlighted in gray. The image name encodes the area, the cell size and the standard deviation of the gaussian filter (eg. M0407 means medium area, cell size 0.4 m and standard deviation 0.7).

Easy area		Medium area		Hard area	
Image	AI (%)	Image	AI (%)	Image	AI (%)
E0300	94.9	M0300	84.5	H0400	64.6
E0305	96.1	M0305	86.2	H0405	65.5
E0306	96.9	M0306	84.7	H0406	67.5
E0307	97.1	M0307	83.6	H0407	67.0
E0308	96.4	M0308	84.3	H0408	67.0
E0309	96.5	M0309	84.5	H0409	67.0
E0310	96.4	M0310	84.0	H0410	65.5
E0400	95.1	M0400	86.2	H0500	67.5
E0405	98.0	M0405	85.9	H0505	70.9
E0406	98.7	M0406	86.2	H0506	71.8
E0407	98.6	M0407	87.6	H0507	68.9
E0408	97.9	M0408	87.8	H0508	73.3
E0409	97.6	M0409	87.1	H0509	68.9
E0410	97.0	M0410	87.8	H0510	69.4
E0500	95.3	M0500	83.8	H0600	70.9
E0505	97.0	M0505	87.6	H0605	70.9
E0506	96.5	M0506	89.2	H0606	71.4
E0507	95.0	M0507	89.9	H0607	69.9
E0508	93.1	M0508	91.1	H0608	72.3
E0509	92.2	M0509	91.8	H0609	72.3
E0510	91.4	M0510	91.8	H0610	73.3

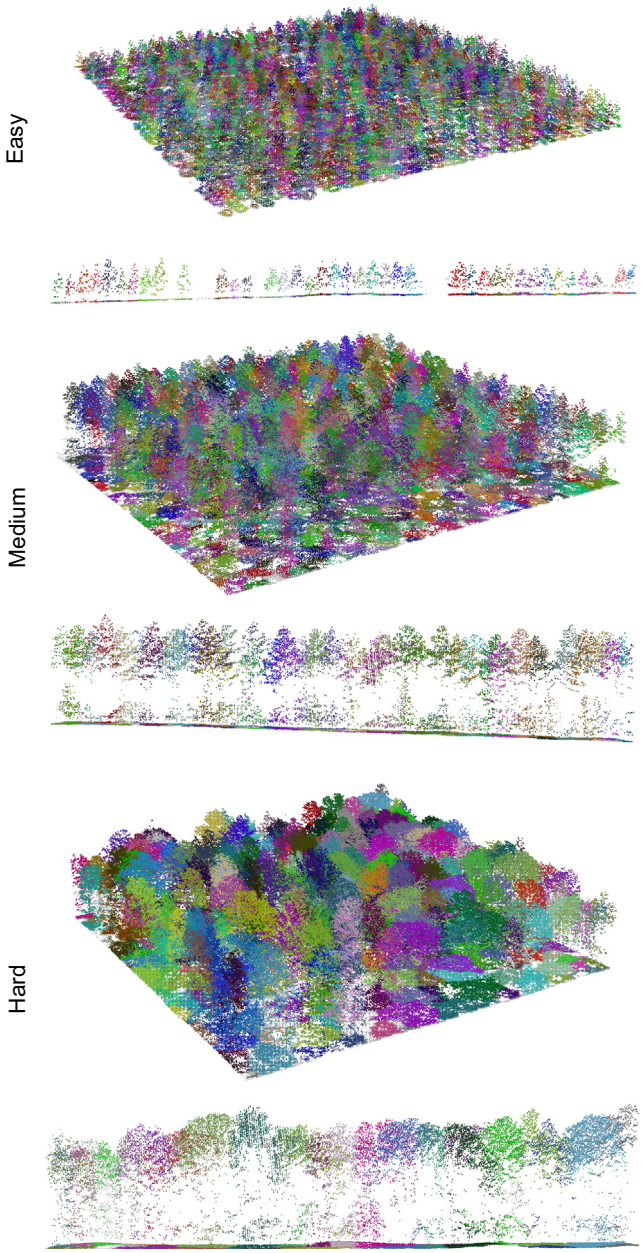

Fig. 11. Segmentation results with individual crowns highlighted in different colors.

Table 3
Results after parameter refinement in the second phase. Omission (O), comission (C), total error ($O + C$) and the number of reference trees (N) are expressed in number of observation and accuracy index (AI) in percent. The detection rate (DR) is reported with respect to three forest layers: lower layer (LL), intermediate layer (IL) and upper layer (UL). Results reported by Reitberger et al. (2009) are also included for comparison.

Area	Stems(ha)	DR/N (LL)	DR/N (IL)	DR/N (UL)	O	C	$O + C$	N	AI (%)
Easy	1380	94.89/130	99.3/858	100/379	13	1	14	1380	98.98
Medium	426	-/0	83.33/30	96.66/377	19	14	33	426	92.25
Hard	206	0/1	66.67/24	88.76/150	32	20	52	206	74.75
Reitberger et al. (2009)	460	21/466	38/374	87/880				1720	51

within the first third of the index values for the easy and medium areas (Fig. 12). A plateau is reached for the hard area after an increase to 40% for all measures, except total error that reaches a plateau after 50%.

With respect to individual cohesion criterion importance, Fig. 13 presents the distribution of AI for results that were obtained using a single criterion (i.e. the weights of the remaining four being set to 0). Irrespective of the area ND induces the largest variation and LD is the best criterion overall when used exclusively. The fitness of the criteria changes with the complexity of the area, with TD and CD being the most appropriate for easy area and LD for the medium and hard area.

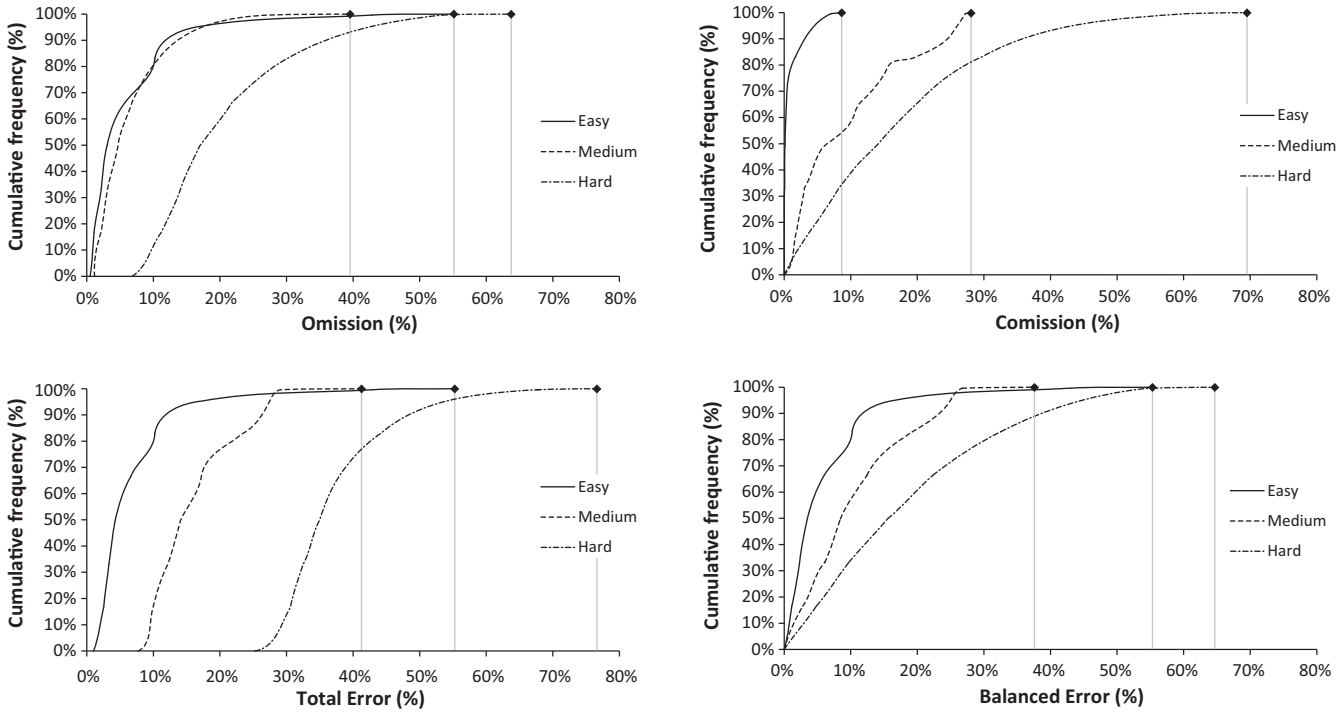

Fig. 12. Cumulated frequency of each accuracy measure in the second phase results for the three areas. Vertical lines mark the last (i.e. worst) accuracy measure value.

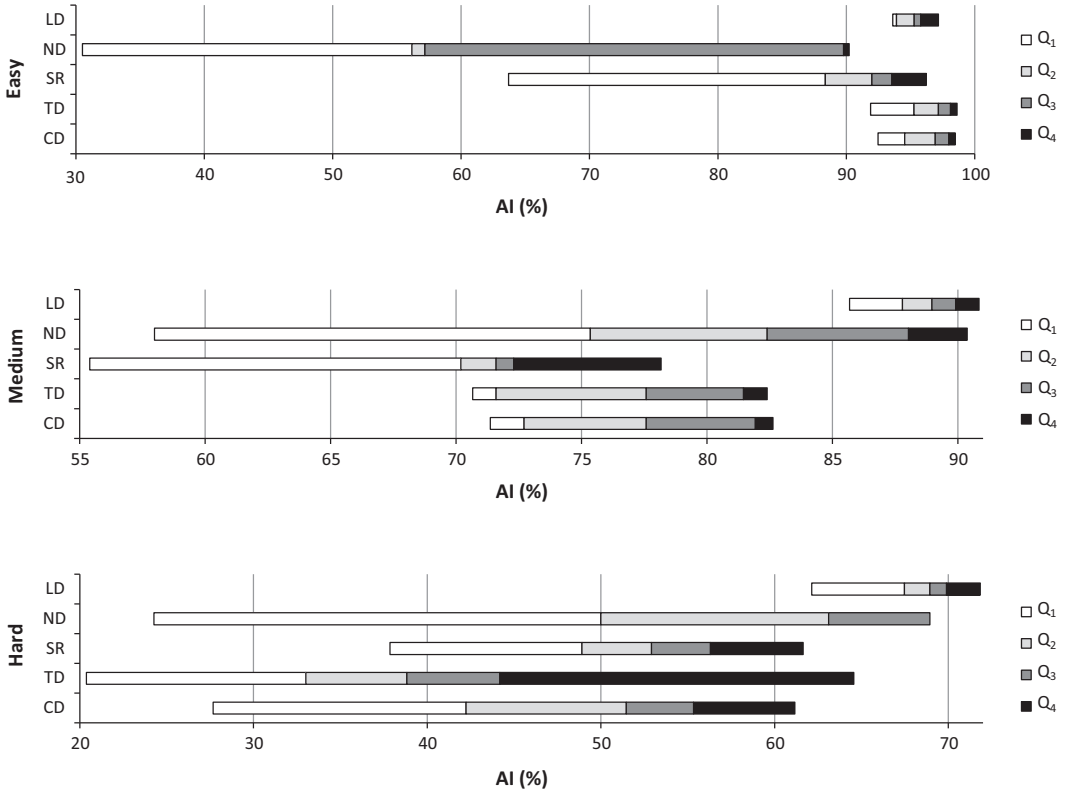

Fig. 13. Distribution box plot of AI values when a single cohesion criterion is used.

ANOVA showed that irrespective of the area each cohesion criterion has a significant impact on AI ($p < 0.001$). The significance level was not necessarily reflected by a large coefficient of correlation, as it varied from 6% (i.e., AI for the hard area) to 35% (i.e., AI for the medium area). Bonferroni multiple comparisons test revealed the existence of criteria weights groups for several consecutive best results (Table 4). For the easy area the best 4 AIs were obtained by similar cohesion criteria weights. For the medium area, the LD and CD criteria show particular consistency in their optimal weights as their first two weight groups span the best 9 AIs. Finally, for the hard area, LD and ND have consistent weights for the best 4 and 5 AIs. These findings not only demonstrate the existence of certain patterns in the cohesion criteria weights yielding quality segmentations, but also show that these patterns are forest condition specific.

When the spectrum of association between cohesion criteria was investigated, ANOVA showed the existence of significant interaction between LD, ND, and SR, as well as between TD and CD, for all three areas ($p < 0.001$). The coefficient of correlation further supported the separation of factors in the ANOVA model, as smallest values were found between LD and ND, and TD and CD. Considering that interaction among criteria affects independent interpretation of each criterion, MANOVA results were used to identify possible sets of criteria leading to superior segmentation. Regardless of the area, the first three eigenvectors were significant ($p < 0.001$), and covered more than 99% of variation (Table 5). However, only the first two eigenvectors were selected for interpretation, as each represents more than 5% of the variation (Table 5). For the easy area the combination SR, ND, and TD provided the best segmentation, followed by the pair LD and ND. For medium area, the association of SR, LD and ND was the most appropriate, followed by the pair ND and SR. The best segmentation for hard area was provided by the combination of LD, ND and TD (Table 5).

When plot data is used to estimate the segmentation parameters, the AI for the easy area ranges from 96.88% to 98.4% (mean $\mu = 97.68\%$) when the 500 m^2 are used and from 97.46% to 98.69% ($\mu = 98.23\%$) when the larger 1000 m^2 are used. These results are quite close to the optimum of 98.98%. For the medium area, the AI ranges from 83.09% to 91.31% ($\mu = 87.78\%$) and from 87.55% to 91.07% ($\mu = 89.24\%$) when the small, respectively the larger plots are used compared to an optimum of 92.25%. The similar AI ranges for the hard area are: 36.4–73.3% ($\mu = 61.1\%$) and 62.13–72.33% ($\mu = 68.04\%$). The difference in AI range for the hard area can be explained by the smaller probability to capture a complex heterogeneous forest structure within a smaller plot.

Irrespective of the study area and plot size t-tests indicate that the AI values obtained with plot information are significantly different from the optimum values. Kolmogorov–Smirnov test support the findings of the t-test, as there was no evidence of non-normal distribution (i.e., $p > 0.1$ for all areas and plot sizes). However, statistical significance, which is induced by the small variability of plot-based results, does not have operational significance for homogeneous stands (i.e., easy and medium areas), as the difference between of plot-based results and optimal result is less than 5% in average. For the heterogeneous stand (i.e. hard area) the average difference is 13.65% when 1000 m^2 plots are used and 6.71% for the 500 m^2 plots.

Table 4
Grouping of weights according to Bonferroni test, executed in respect to an individual cohesion criterion. Same letter indicates similar weight values, while a different letter delineates significantly different weight values.

Area	Weight	Departure from minimum total errors									
		0	1	2	3	4	5	6	7	8	9
Easy	LD	A	A	A	A	B	C	D	E	F	G
	ND	A	A	A	A	B	C	D	D	D	D
	SR	A	A	A	A	B	C	D	E	E	F
	TD	A	A	A	A	B	C	D	D	D	E
	CD	A	A	A	A	A	A	B	B	B	B
Medium	LD	A	A	A	A	A	B	B	B	C	D
	ND	A	B	C	D	E	F	F	G	H	I
	SR	A	A	A	B	C	D	E	F	G	H
	TD	A	A	B	C	D	D	D	E	F	G
	CD	A	B	B	B	B	B	B	B	B	C
Hard	LD	A	A	A	A	B	C	D	D	E	E
	ND	A	A	A	A	A	B	C	D	E	E
	SR	A	A	B	C	D	E	F	G	H	H
	TD	A	A	B	C	D	D	E	F	F	F
	CD	A	A	B	C	C	D	D	D	E	E

4. Discussion

4.1. Comparison with a similar study

Allowing that algorithm performance comparison may be difficult if applied on different forest conditions (Vauhkonen et al., 2012), we identified Reitberger et al. (2009) as a somewhat appropriate study for comparison with our hard area due to the similar forest condition (leaf-off mixed mature forest), acquisition parameters (Riegl scanner, ~25 Pts/m^2) and assessment criteria, specifically in terms of forest layer definition. While the detection rate in the upper layer is similar, with 88.76% in our hard area and 87% in Reitberger's (Table 3), in the intermediate layer we have detected 66.67% of the trees compared to only 38% reported by Reitberger. Overall, in terms of AI our method outperformed Reitberger's by 23% (i.e. Reitberger had an AI = 51% as calculated by subtracting the false positives percentage of 9% from the DR = 60%). It must be noted however, that Reitberger's forest had a mean stem density of 460 stems/ha with only 14% of the total forest area with a density of 200 trees/ha or lower, and a significant portion of trees (=27%) in

Table 5
MANOVA for identification of the cohesion criteria leading to superior segmentation (*represents criteria related to the eigenvector).

Area	Eigenvector	Proportion variation	Cumulative variation	Standardized coefficients				
				LD	ND	SR	TD	CD
Easy	1	0.92	0.92	−0.17	−0.43*	−0.62*	−0.58*	0.00
	2	0.06	0.98	0.82*	−0.35*	−0.24	0.24	0.00
	3	0.001	0.98	0.96	1.01	0.79	0.70	0.00
Medium	1	0.78	0.78	0.50*	0.37*	0.59*	−0.25	0.00
	2	0.20	0.98	0.21	−0.54*	0.67*	−0.17	0.00
	3	0.02	0.99	0.77	0.65	−0.12	−0.51	0.00
Hard	1	0.85	0.85	0.84*	1.07*	−0.11	0.77*	0.00
	2	0.09	0.94	−0.32*	0.64*	0.16	−0.36*	0.00
	3	0.05	0.99	0.55	−0.04	−0.16	−0.73	0.00

the lower forest layer. Our hard area compensates the low density with two properties that endorse its difficulty:

- *Extensive oak crowns*. The water oak species of Louisiana are fast growing, and their crowns span diameters >10 m at maturity. These crown shapes are very irregular and prone to over segmentation, especially in leaf-off condition.
- *Compact tree clusters*. Tree crowns of different shapes and heights that are clumped together are difficult to separate.

These structural forest properties that hamper the segmentation also explain the relative low stem density, as the large oak crowns span large horizontal regions and the crown clusters are sometimes separated by gaps, decreasing hence the mean density.

4.2. Particular aspects related to parameterization

The power of the present segmentation method equates to the flexible parameterization that relates local structures in a topologically meaningful way. If we were to consider the hyper-surface of accuracy in the hyper-space of parameters when segmenting a certain forest area, the proposed approach produces a surface that despite having a complicated shape gets significantly close to a global optimum in some areas. In other words, it has substantial potential given the right parameterization. On the downside, finding a good parameterization is not trivial as the parameters are rather abstract and their interaction counterintuitive. To address this aspect we investigate the possibility to tune the parameters using plot data. The results suggest that if the forest area of interest is sufficiently homogenous, the parameters derived from segmentation in a certain plot could estimate the optimum parameterization globally (See Fig. 14).

Successful parameter extrapolation from area plot to the entire forest suggests that indeed the cohesion criteria weights, as core parameters, indirectly characterize a specific forest structure. To demonstrate this important assumption, we have analyzed the criteria weight distributions for those parameterizations that have resulted in quality segmentations.

MANOVA identified the combination of cohesion criteria that can supply superior overall segmentation results, but did not indicate which set of criteria lead to superior results. To complement MANOVA findings, the evolution of weights for each criterion was presented in respect with the number of errors (Fig. 15). The cumulated mean cohesion criteria weights showed that the smallest number of errors for easy area was obtained using only ND and TD, while best 10 results were obtained by the combination of ND, SR, and TD, in agreement with MANOVA. For medium area, LD, ND and SR supplied the best results, combination valid also for best 10 results. For hard area, LD, ND and TD lead to the best results and the subsequent 9, substantiating MANOVA results. The set of criteria leading to reduced number of errors differs with complexity of the area, which suggests that prior assessment of the area will likely produce superior segmentations.

The results of Bonferroni test, which indicated that criteria weights impact differently the performance of the algorithm, were supplemented by the mass density function of the weights of each cohesion criterion (Fig. 16), which revealed a bimodal distribution

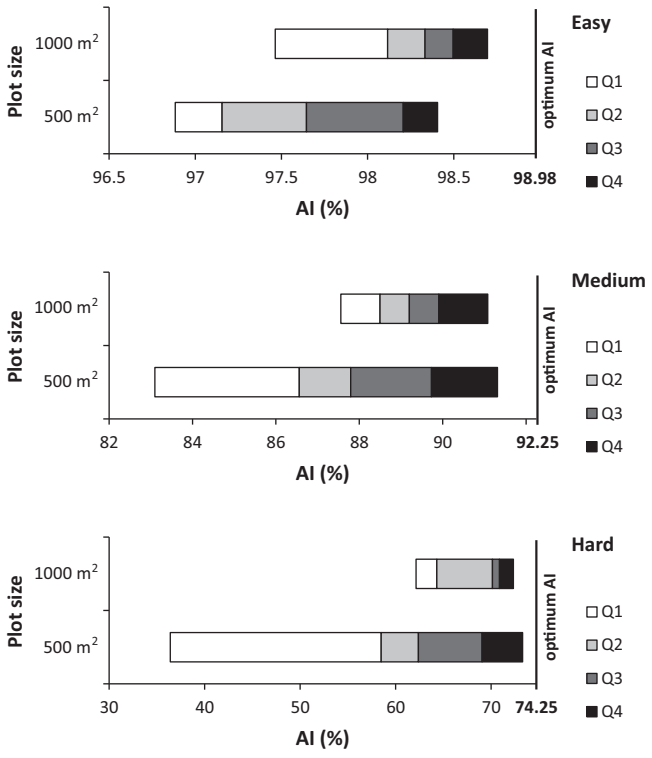

Fig. 14. Distribution of AI values when the parameters are estimated by plots. Q1 through Q4 represent inter-percentile ranges.

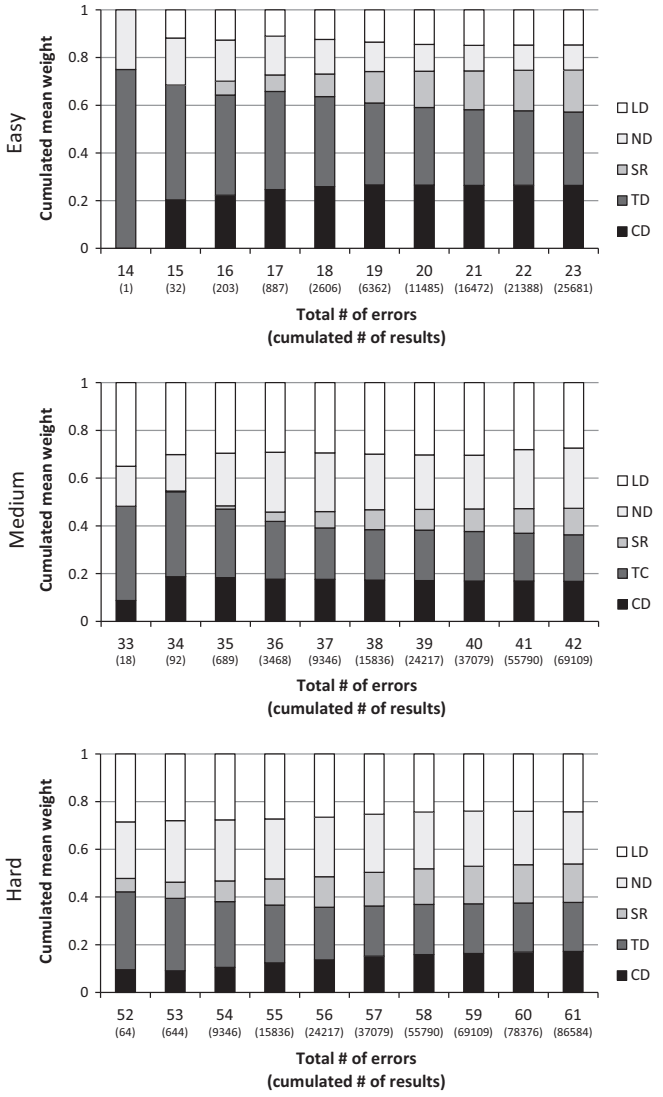

Fig. 15. Cumulated mean cohesion criteria weights for results within 10 errors from the best in each area.

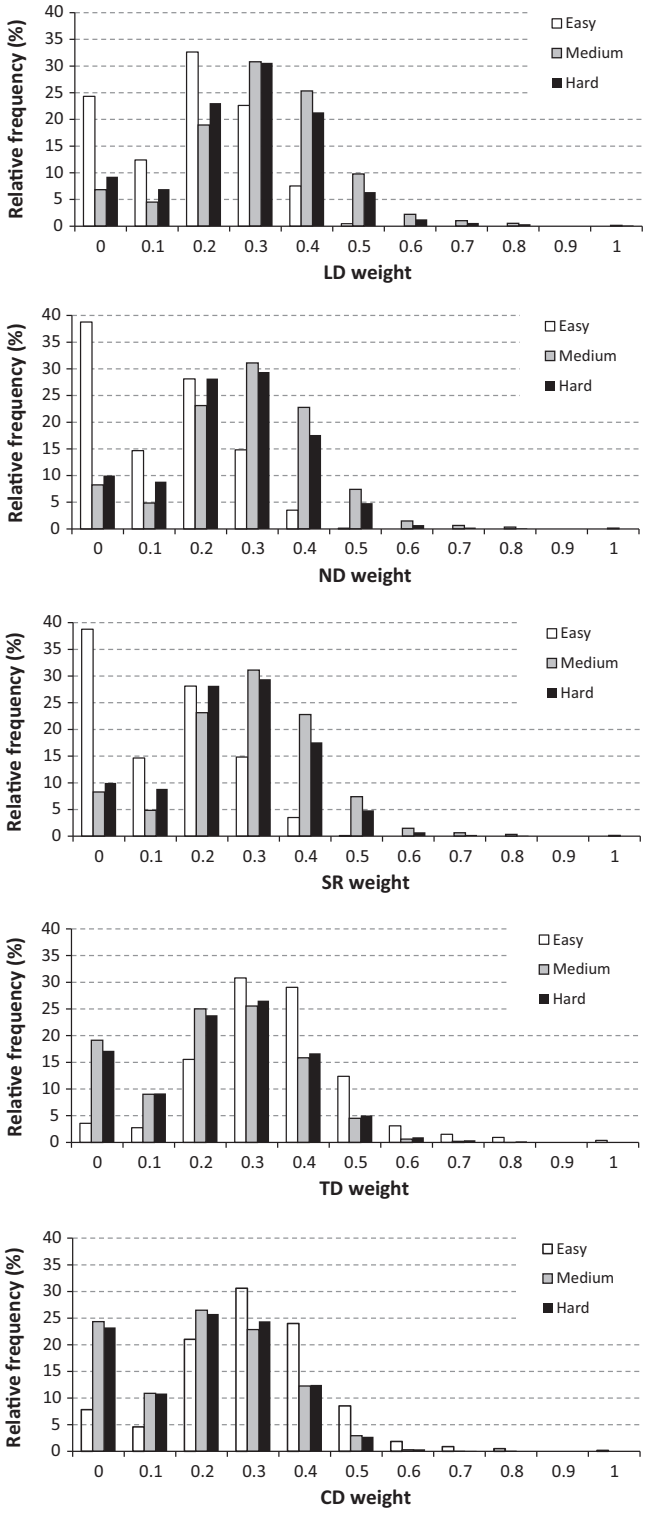

Fig. 16. Mass density function of weights for each cohesion criterion for the best 10 AIs obtained in each area.

with one mode around 0, and one around 0.3. The concentration of weight around 0 for easy area of criteria measuring hierarchy (i.e., LD, ND and SR) confirms that these criteria should be used in combination, not alone, which is the conclusion of MANOVA. For medium and hard areas, measures of real distances seem to be of little value when considered alone, again confirming MANOVA. The second mode, considered in the light of MANOVA, recommends the range of weights of each criterion, which is between 0.2 and 0.4, in agreement with the cumulated mean cohesion criteria weights for best 10 results. Therefore, for areas of little complexity, the cohesion criteria to be used are SR, ND, and TD, with weights around 0.3 (e.g., SR could be 0.4). For areas with medium complexity, the criteria operating only on the hierarchy suffice (i.e., ND, LD, and SR), with weight 0.3 (e.g., SR also 0.4). For hard areas, the combination of ND, LD, and TD lead to the best results, with weight approximately 0.3 (e.g., ND can be 0.4).

4.3. Segmentation framework and perspective

Beyond developing an efficient segmentation method, we created a powerful framework that has the potential to support a series of graph theoretical algorithms. We describe a hierarchized data structure that captures and organizes the topological structure of a forest and provides support for a wide range of procedures including but not limited to segmentation algorithms. For instance, calculating an average drop in levels between any two parent–child patches in the hierarchy may be an indication of the tree species composition of the forest area. Coniferous trees tend to have cone shaped crowns that are rather steep and will result in a more abrupt level drop for adjacent patches.

In terms of segmentation algorithms, the hierarchies and the weighted graph provide an efficient support for several traditional segmentation methods to be reproduced in this framework. For instance, a region growing algorithm may be reduced to our framework by enforcing a stopping criteria based on a relation between LD and ND (i.e. big LD and small ND between two locations indicate an abrupt valley). Valley following algorithms may be reduced to following the set of contact patches that exists between hierarchies. Local maxima based segmentation is realized by using TD criteria exclusively in the edge weight calculation. Global optimization algorithms may be realized by partitioning the weighted graph in a way that minimizes an appropriate objective function. Even template matching methods may find support in the proposed framework if the target model has an equivalent definition as a graph theoretical structure.

Several improvements have been considered for further investigation. In terms of graph partitioning, hierarchical clustering may avoid over- and under-segmentation by choosing an appropriate level in the dendrogram. An additional cohesion criterion like the shape index used by Bunting and Lucas (2006) may evaluate whether the union of two hierarchy patches lays out in a geometry that completes a tree. The potential of a shape index can be better exploited if the simple oriented graph is replaced by a hypergraph, allowing an edge to connect more than two nodes. Calculating weights for the hyperedges would use modified versions of the cohesion criteria. Multiple hierarchies connected by a hyperedge would yield a high response to the shape index if in reality they form a complete tree. In a sense, situations where more than two hierarchies form a complete tree would be better accounted for and rewarded with a high score for the shape index and other generalized cohesion criteria.

A particular quality of graph-based methods is the potential to parallelize the computational work by partitioning the graph, processing the partitions in parallel, and finally stitching together the result. Wassenberg et al. (2009) proposed a parallelization method for graph-based image segmentation that does not truncate objects located at partition boundaries. Considering that remotely sensed data for entire forests is usually quite large, the potential to parallelize the segmentation process is a significant advantage.

5. Conclusion

We present here a novel graph-theoretical approach to tree crown delineation. While major tree crown components are easily

identified by local maxima, deciding the subsets that form integral crowns is not trivial. Addressing this observation, we developed a methodology to assess the cohesion between crown components and subsequently identify groups of highly cohesive components. The spatial data is organized hierarchically by height and a weighted mean of several quantifiable cohesion criteria secures the flexibility that allows the algorithm to adjust to different data sets. The low omission and commission rates for three structurally different forest areas recommend the proposed algorithm as an excellent segmentation procedure with proved ability to adapt to varied forest conditions.

The current platform-like implementation embodies substantial potential for enhancement, particularly in terms of integrating new cohesion criteria and graph clustering procedures. This quality together with the already existent flexibility will allow robust segmentation methodologies to be tailored for any kind of topological data, thus extending the algorithm application to other fields.

Acknowledgments

This work was supported by the Louisiana Board of Regents Grant number LEQSF(2012-15)-RD-B-04, and UEFSCDI project No. PN-II-PT-PCCA-2011-3.2-1710.

References

Bottai, L., Arcidiaco, L., Chiesi, M., Maselli, F., 2013. Application of a single-tree identification algorithm to LiDAR data for the simulation of stem volume current annual increment. J. Appl. Remote Sens. 7, 073699.

Brandtberg, T., Warner, T.A., Landenberger, R.E., McGraw, J.B., 2003. Detection and analysis of individual leaf-off tree crowns in small footprint, high sampling density lidar data from the eastern deciduous forest in North America. Remote Sens. Environ. 85, 290–303.

Bunting, P., Lucas, R., 2006. The delineation of tree crowns in Australian mixed species forests using hyperspectral Compact Airborne Spectrographic Imager (CASI) data. Remote Sens. Environ. 101, 230–248.

Culvenor, D.S., 2002. TIDA: an algorithm for the delineation of tree crowns in high spatial resolution remotely sensed imagery. Comput. Geosci. 28, 33–44.

Daliakopoulos, I.N., Grillakis, E.G., Koutroulis, A.G., Tsanis, I.K., 2009. Tree crown detection on multispectral VHR satellite imagery. Photogramm. Eng. Remote Sens. 75, 1201–1211.

Dralle, K., Rudemo, M., 1996. Stem number estimation by kernel smoothing of aerial photos. Can. J. For. Res. 26, 1228–1236.

Ene, L., Næsset, E., Gobakken, T., 2012. Single tree detection in heterogeneous boreal forests using airborne laser scanning and area-based stem number estimates. Int. J. Remote Sens. 33, 5171–5193.

Erikson, M., 2003. Segmentation of individual tree crowns in colour aerial photographs using region growing supported by fuzzy rules. Can. J. For. Res. 33, 1557–1563.

Forzieri, G., Guarnieri, L., Vivoni, E.R., Castelli, F., Preti, F., 2009. Multiple attribute decision making for individual tree detection using high-resolution laser scanning. For. Ecol. Manage. 258, 2501–2510.

Gebreslasie, M.T., Ahmed, F.B., Van Aardt, J.A.N., Blakeway, F., 2011. Individual tree detection based on variable and fixed window size local maxima filtering applied to IKONOS imagery for even-aged Eucalyptus plantation forests. Int. J. Remote Sens. 32, 4141–4154.

Gougeon, F.A., Moore, T., 1989. Classification individuelle des arbres à partir d'images à haute résolution spatiale, pp. 185–196.

Gougeon, F., Leckie, D., Gillis, M., 1992. Individual tree identification from high resolution MEIS images. In: International Forum on Airborne Multispectral Scanning for Forestry and Mapping. Quebec: Petawawa National Forestry Institute, Forestry Canada, pp. 117–128.

Gupta, S., Weinacker, H., Koch, B., 2010. Comparative analysis of clustering-based approaches for 3-D single tree detection using airborne fullwave lidar data. Remote Sensing 2, 968–989.

Hardle, W., Simar, L., 2003. Applied Multivariate Statistical Analysis. Springer-Verlag, New York.

Heinzel, J.N., Weinacker, H., Koch, B., 2011. Prior-knowledge-based single-tree extraction. Int. J. Remote Sens. 32, 4999–5020.

Hengl, T., 2006. Finding the right pixel size. Comput. Geosci. 32, 1283–1298.

Hirschmugl, M., Ofner, M., Raggam, J., Schardt, M., 2007. Single tree detection in very high resolution remote sensing data. Remote Sens. Environ. 110, 533–544.

Holmgren, J., Persson, Å., 2004. Identifying species of individual trees using airborne laser scanner. Remote Sens. Environ. 90, 415–423.

Horváth, P., Jermyn, I., Kato, Z., Zerubia, J., 2006. A higher-order active contour model of a 'gas of circles' and its application to tree crown extraction. In: Kalra, P., Peleg, S. (Eds.), Computer Vision, Graphics and Image Processing. Springer, Berlin Heidelberg, pp. 152–161.

Hung, C., Bryson, M., Sukkarieh, S., 2012. Multi-class predictive template for tree crown detection. J. Photogramm. Remote Sens. 68, 170–183.

Hyyppä, J., Hyyppä, H., Inkinen, M., Engdahl, M., Linko, S., Zhu, Y.-H., 2000. Accuracy comparison of various remote sensing data sources in the retrieval of forest stand attributes. For. Ecol. Manage. 128, 109–120.

Jakubowski, M.K., Li, W., Guo, Q., Kelly, M., 2013. Delineating individual trees from lidar data: a comparison of vector- and raster-based segmentation approaches. Remote Sensing 5, 4163–4186.

Kaartinen, H., Hyyppä, J., Yu, X., Vastaranta, M., Hyyppä, H., Kukko, A., Holopainen, M., Heipke, C., Hirschmugl, M., Morsdorf, F., Næsset, E., Pitkänen, J., Popescu, S., Solberg, S., Wolf, B.M., Wu, J.-C., 2012. An international comparison of individual tree detection and extraction using airborne laser scanning. Remote Sensing 4, 950–974.

Kwak, D.-A., Lee, W.-K., Lee, J.-H., Biging, G., Gong, P., 2007. Detection of individual trees and estimation of tree height using LiDAR data. J. For. Res. 12, 425–434.

Larsen, M., Rudemo, M., 1998. Optimizing templates for finding trees in aerial photographs. Pattern Recogn. Lett. 19, 1153–1162.

Larsen, M., Eriksson, M., Descombes, X., Perrin, G., Brandtberg, T., Gougeon, F., 2011. Comparison of six individual tree crown detection algorithms evaluated under varying forest conditions. Int. J. Remote Sens. 32, 5827–5852.

Lee, H., Slatton, K.C., Roth, B.E., Cropper, W.P., 2010. Adaptive clustering of airborne LiDAR data to segment individual tree crowns in managed pine forests. Int. J. Remote Sens. 31, 117–139.

Liu, J., Shen, J., Zhao, R., Xu, S., 2013. Extraction of individual tree crowns from airborne LiDAR data in human settlements. Math. Comput. Modell. 58, 524–535.

Næsset, E., 1997. Estimating timber volume of forest stands using airborne laser scanner data. Remote Sens. Environ. 61, 246–253.

Næsset, E., 2002. Predicting forest stand characteristics with airborne scanning laser using a practical two-stage procedure and field data. Remote Sens. Environ. 80, 88–99.

Noble, R., Smith, E.P., Ye, K., 2004. Model selection in canonical correlation analysis (CCA) using Bayesian model averaging. Environmetrics 15, 291–311.

Palenichka, R., Zaremba, M., 2007. Scale-adaptive segmentation and recognition of individual trees based on LiDAR data. In: Kamel, M., Campilho, A.I. (Eds.), Image Analysis and Recognition. Springer, Berlin Heidelberg, pp. 1082–1092.

Palenichka, R., Doyon, F., Lakhssassi, A., Zaremba, M.B., 2013. Multi-scale segmentation of forest areas and tree detection in LiDAR images by the attentive vision method. Selected Topics Appl. Earth Observ. Remote Sens., IEEE J. 6, 1313–1323.

Persson, A., Holmgren, J., Soderman, U., 2002. Detecting and measuring individual trees using airborne laser scanning. Photogramm. Eng. Remote Sens. 68, 925–932.

Pirotti, F., 2010. Assessing a template matching approach for tree height and position extraction from lidar-derived canopy height models of pinus pinaster stands. Forests 1, 194–208.

Pitkänen, J., 2001. Individual tree detection in digital aerial images by combining locally adaptive binarization and local maxima methods. Can. J. For. Res. 31, 832–844.

Popescu, S.C., Wynne, R.H., 2004. Seeing the trees in the forest: using lidar and multispectral data fusion with local filtering and variable window size for estimating tree height. Photogramm. Eng. Remote Sens. 70, 589–604.

Pouliot, D.A., King, D.J., Bell, F.W., Pitt, D.G., 2002. Automated tree crown detection and delineation in high-resolution digital camera imagery of coniferous forest regeneration. Remote Sens. Environ. 82, 322–334.

Reitberger, J., Schnörr, C., Krzystek, P., Stilla, U., 2009. 3D segmentation of single trees exploiting full waveform LIDAR data. J. Photogramm. Remote Sens. 64, 561–574.

Rencher, A.C., 1992. Interpretation of canonical discriminant functions, canonical variates, and principal components. Am. Stat. 46, 217–225.

SAS Institute, 2010. SAS. In: Cary NC: SAS Institute.

Skurikhin, A.N., Garrity, S.R., McDowell, N.G., Cai, D.M., 2013. Automated tree crown detection and size estimation using multi-scale analysis of high-resolution satellite imagery. Remote Sens. Lett. 4, 465–474.

Tabachnick, B.G., Fidell, L.S., 2001. Using multivariate statistics. Needham Heights: Allyn and Bacon.

Tang, F., Zhang, X., Liu, J., 2007. Segmentation of tree crown model with complex structure from airborne LIDAR data. pp. 67520A-67520A-67529.

Tittmann, P., Shafii, S., Hartsough, B., Hamann, B., 2012. Tree Detection and Delineation from LiDAR point clouds using RANSAC.

Vauhkonen, J., Ene, L., Gupta, S., Heinzel, J., Holmgren, J., Pitkänen, J., Solberg, S., Wang, Y., Weinacker, H., Hauglin, K.M., Lien, V., Packalén, P., Gobakken, T., Koch, B., Næsset, E., Tokola, T., Maltamo, M., 2012. Comparative testing of single-tree detection algorithms under different types of forest. Forestry 85, 27–40.

Wassenberg, J., Middelmann, W., Sanders, P., 2009. An efficient parallel algorithm for graph-based image segmentation. In: Jiang, X., Petkov, N. (Eds.), Computer Analysis of Images and Patterns. Springer, Berlin Heidelberg, pp. 1003–1010.

Wolf, B.-M., Heipke, C., 2007. Automatic extraction and delineation of single trees from remote sensing data. Mach. Vis. Appl. 18, 317–330.

Wulder, M., Niemann, K.O., Goodenough, D.G., 2000. Local maximum filtering for the extraction of tree locations and basal area from high spatial resolution imagery. Remote Sens. Environ. 73, 103–114.

Yu, X., Hyyppä, J., Vastaranta, M., Holopainen, M., Viitala, R., 2011. Predicting individual tree attributes from airborne laser point clouds based on the random forests technique. J. Photogramm. Remote Sens. 66, 28–37.

Zhang, J., Sohn, G., 2010. A Markov Random Field Model for Individual Tree Detection from Airborne Laser Scanning Data, pp. 120–125.